Angular, energy and charge distribution in the scattering of low-energy helium ions by an amorphous silicon surface

1998 J. Phys.: Condens. Matter 10 741

(http://iopscience.iop.org/0953-8984/10/4/004)

J. Phys.: Condens. Matter **10** (1998) 741–752. Printed in the UK PII: S0953-8984(98)84520-7

Angular, energy and charge distribution in the scattering of low-energy helium ions by an amorphous silicon surface

B Arezki†, Y Boudouma†, P Benoit-Cattin‡, A C Chami†, C Benazeth‡, K Khalal† and M Boudjema†‡

† Institut de Physique, USTHB, BP32 El Alia, Bab Ezzouar, Alger, Algeria
‡ LCAR–IRSAMC, UMR 5589 Université Paul Sabatier–CNRS, 31062 Toulouse Cédex, France

Received 27 May 1997, in final form 30 October 1997

Abstract. We have performed an experimental investigation of the angular distribution of LEIS spectra and the charge fraction for the 4 keV He^+/a:Si system at 6 and 20° of incidence angle. A numerical model is developed in order to assure a quick adjustment of several parameters. The influence of the electronic stopping power, the charge exchange in close collisions, the Auger neutralization, the expansion of electronic density outside the bulk and the image charge effect are studied and discussed. A good agreement is found between the experimental results and the numerical calculation.

1. Introduction

In the last ten years, increasing interest has appeared in the low-energy ion spectroscopy technique (LEIS) to determine both elemental composition and structure of solid surfaces. In particular, as well established now by several works ([1] and references therein), processes like the charge exchange and the inelastic energy loss play an important part and are strongly dependent on surface state. Therefore, the understanding of such mechanisms becomes essential to allow a quantitative interpretation by accurate numerical simulation of ion and neutral scattering spectra. This is the aim of our present work for 4 keV He^+/a:Si collision.

Many features of charge exchange near the surface are beginning to be qualitatively well understood. For instance, it has been found that variation of the ion survival probability follows the well known Hagstrum adiabatic model [2] for Auger and resonant neutralization. This model, initially developed for very low incident energy (eV range), has been quite successfully extended to the keV region [3]. However, the increase of incident energy (and so the decrease of distance of closest approach) leads to the appearance of charge exchange in close collision. This is a threshold phenomenon [4–7] correctly explained by the so-called electron promotion model in the quasi-molecule frame [8]. Occurrence of neutralization and reionization in close encounter has been clearly shown by the similar charge fraction obtained by the use of both neutral and ionic projectiles at quite grazing incidence angle [9, 10]. But, despite a few investigations [11, 12], the weight of this mechanism remains poorly known.

Beside this, LEIS experiments may be also a useful way to measure the electronic stopping power in the low-velocity range (below 1 au). This can be performed either by measuring the shift of scattered particle energy with respect to their elastic position

0953-8984/98/040741+12$19.50

value [4] or by using the stopping power as a fit parameter in a computer simulation. This latter method has been used in an analytical formulation by Närmann *et al* [13] under the following assumptions: (i) the shape of scattering spectra is only due to Auger neutralization and to the difference between stopping power of ionic and neutral species, (ii) the multiple-scattering events and the possibility of charge exchange at very short collision distance are disregarded. The result is a large overestimation of the ionic stopping power. A more realistic approach taking also into account the occurrence of multiple scattering and the two main processes of charge exchange cannot be achieved analytically. It requires a numerical simulation. The Monte Carlo method is currently used for this goal in simulation codes such as MARLOWE [14] and TRIM [15]. Unfortunately, owing to the large time they need, they are inappropriate to fit experimental results by adjustment of several parameters as we want to do here. Indeed, in this work, the Auger neutralization rate, close neutralization and reionization probability, threshold impact parameter, expansion of the electronic density outside the bulk and stopping power are all considered as parameters to fit the scattered spectra and the angular distribution of charge fraction.

Thus, we present in this paper a numerical procedure based on a modified TRIM code allowing such adjustment. The simulated spectra and the angular distribution of charge fraction are compared to the experimental ones. This is done in section 4 with some theoretical considerations about the stopping power calculations. The obtained parameter values are discussed in section 5. The main aspects of the charge exchange processes (Auger neutralization and close encounter transition probabilities) are presented in section 3. Before that, the experimental set-up is briefly described in section 2. Unless otherwise specified, we use the Hartree atomic units ($e = m = \hbar = 1$).

2. Experiment

The experimental part of this work was performed on the apparatus already described elsewhere [16]. The main features can be summarized as follows. A discharge source (Colutron type), with a 4 kV extraction voltage, provides ions from an He–Ne gas mixture. After sorting in a Wien filter, pulsing and focusing by Einzel lenses, the He^+ beam enters the UHV analysis chamber (residual pressure of about 10^{-9} Torr). It collides with an amorphous silicon target mounted on a sample manipulator–goniometer system with five degrees of freedom (X, Y, Z, polar and azimuthal angles). The incidence angle α (relative to the sample surface) is able to vary from the normal direction to the grazing one.

The scattered particles are post-accelerated by a few kV grid voltage along a short distance. They are analysed by a time of flight (TOF) spectrometer according to their charge state. After deceleration to their initial energy, they are detected by a two-stage micro-channel plate. The TOF spectrometer can rotate around the centre of collision so that the detection angle θ varies continuously from 0 to 165° relative to the incident beam direction.

In order to control the cleanliness of the target surface (especially to remove hydrogen deposits), periodic sputtering by a non-pulsed Ne^+ beam is performed under a quite small incidence angle (10–15°). The average intensity of the He^+ pulsed beam used in this work is about a hundred pA. The TOF spectra recorded for the direct pulsed beam is nearly Gaussian with FWHM of about 20–30 ns at 4 keV. This shape can be assumed as the apparatus function resulting from convolution of initial pulse duration and resolution of the detection system.

3. Charge exchange processes

3.1. Auger neutralization

It has been established that the Auger neutralization is the dominant process of charge exchange in our situation [17, 18]. This process has been already described [2]. The main result is that for slow projectiles travelling near a solid surface, the ion survival probability can be expressed as:

$$P^+ = \exp\left(-\frac{v_c}{v_\perp}\right) \tag{1}$$

where $v_\perp$ is the normal component of the projectile velocity and v_c is a constant which depends on the projectile–target system.

More recently, Lorente *et al* [19] take into account the lowering of the electron barrier at the solid surface as a result of the projectile vicinity. Correspondingly, the electron can freely escape the surface barrier up to a distance d with the constant electronic density of the bulk. One assumes that, beyond d, the electronic density $n(z)$ decreases exponentially as the normal distance z from the surface increases. Using a local approximation for the Auger transition rate τ^{-1}, they mainly show that this rate can be written as:

$$\tau(z) \propto n^{-2}(z). \tag{2}$$

Their results for all values of z can be approximated by:

$$\begin{cases} \tau(z) = \tau_0 \exp((z-d)/a) & \text{for } z > d \\ \tau(z) = \tau_0 & \text{for } z < d. \end{cases} \tag{3}$$

τ_0^{-1} corresponds to the transition rate in the solid bulk characterized by a constant density n_0 of free electrons. The constant a is a characteristic length describing the electronic density decay outside the solid ($z > d$). The local mean length of Auger neutralization $\lambda(z)$ is defined by:

$$\lambda(z) = v\tau(z) \qquad \text{and} \qquad \lambda_0 = v\tau_0. \tag{4}$$

The ion survival probability P^+ is deduced from the general expression $P^+ = \exp(-\int \mathrm{d}t/\tau)$ [2] for the input and output phases:

$$\begin{cases} P^+_{in} = \exp(-(a+d)/\lambda_0 \sin\alpha) \\ P^+_{out} = \exp(-(a+d)/\lambda_0 \sin\beta) \end{cases} \tag{5}$$

where $\beta = \theta - \alpha$ is the exit angle.

3.2. Close-collision neutralization and ionization

Another important mechanism of charge exchange between the projectile and the solid can occur when electronic clouds of the two partners (He and Si) interpenetrate forming a quasi-molecule. The crossing of some levels can lead to an excitation or an ionization in the outgoing channel [8]. This phenomenon has been studied largely in atomic collisions and literature is abundant in this field. For the case of scattering of He by Si, it has been shown by Shoji *et al* [4] that an amount of emerging ions comes from ionization during close collisions at a crossing distance of about 0.35 Å. At the same time, Muda and Newns [20] compute the hopping matrix based on the dynamical calculation on the projectile target correlation. They deduce a close-collision ionization probability of about 10%.

The probability p for remaining in a given state during level crossing is expressed by the Landau–Zener formula:

$$p = \exp(-v_1/v_r(R_c)) \tag{6}$$

where $v_r(R_c)$ is the relative velocity of the two partners at the crossing distance R_c and v_1 is a characteristic velocity which depends on the crossing levels. We use the value $v_1 = 4 \times 10^5$ m s^{-1} given by Beuken and Bertrand [12].

The probabilities of ionization P_I and neutralization P_N during the close collision are assumed to be equal [12] and can be expressed as:

$$P_I = P_N = 2p(1 - p). \tag{7}$$

The $P_I = P_N = P$ hypothesis is valid for a single crossing level and when the electron transfer occurs at the same crossing point for both capture and loss processes.

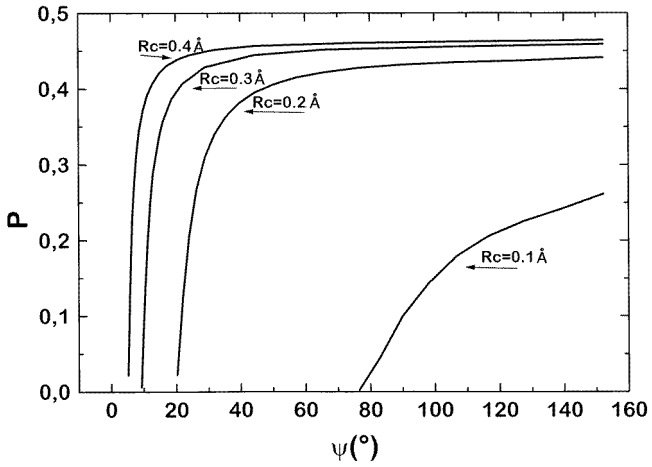

Figure 1. Probability of charge exchange in a close collision following Landau–Zener formula ((7) with $v_1 = 4 \times 10^5$ m s^{-1} [12]) for various crossing distances at 4 keV incident energy.

We have used the well known ZBL potential for He^0/Si collision (neutral–neutral interaction) [15] to compute $V_r(R_c)$ for various impact parameters. The impact parameters are linked to the individual diffusion angle ψ through the used scattering potential. The resulting probability P is shown in figure 1 for various crossing distances. It appears that for $R_c \approx 0.35$ Å, P can be fairly well approximated by a step function Θ as:

$$P = P_0\Theta(\psi - \psi_c) \tag{8}$$

where ψ_c is a critical scattering angle above which charge exchange occurs with a probability P_0. We assume that a similar step function describes the charge exchange probability for He^+/Si collision (ion–neutral interaction). The two values ψ_c and P_0 will be used as adjustable parameters.

4. Numerical procedure

4.1. Monte Carlo description of ion trajectory

At low energy, the projectile emerges from the solid after a sequence of multiple collisions. Angular distribution of scattered particles have been studied in detail in the frame of the

transport theory [21]. Unfortunately, this work concerns transmission through solid targets and is restricted to low scattering angles. Such a study is not available for reflected particles on a thick target and for any scattering angle. For this purpose, we describe the multiple-scattering path by a Monte Carlo code. The general procedure is that given in the TRIM code [15] using the so-called ZBL potential. This code is modified to provide the angular distribution of the scattered particles [22]. To test the validity of the used potential, the angular distribution of experimental total yield (ions + neutrals) is compared with the simulated one. The result shown in figure 2 exhibits an excellent agreement. If we notice that the total yield is independent of the charge state and the stopping power value, this agreement confirms the validity of the ZBL potential in our experimental conditions.

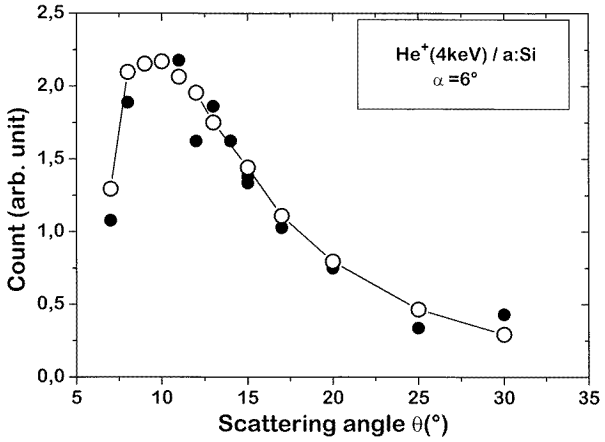

Figure 2. Angular distribution of the scattered particles ($He^0 + He^+$). The theoretical curve (open circles) is normalized to the experimental one (full circles) at the scattering angle $\theta = 10^\circ$.

Two other distributions can also be provided by the modified TRIM code. The first one is the total-length L distribution of the projectile and the second is the individual scattering angle ψ distribution for each collision during the multiple-scattering sequence (figure 3). We remark that, for large scattering angles, the mean path is larger and multiple scattering is more probable. We also deduce from the angular distribution the probability $\Phi(n_c, L)$ of obtaining n_c close collisions during the path length L. A close collision is defined here as collision leading to a single scattering angle $\psi > \psi_c$. These distributions are performed once and for all to be used as input to the adjustment model.

4.2. Charge exchange in the bulk

For a given value of n_c, the ith close collision occurs after a total path length x_i in the solid, so that the condition $x_1 < x_2 < \cdots < x_i < \cdots < x_{nc}$ holds.

Let P_{in}^+ and $P_{in}^0 = 1 - P_{in}^+$ be the ionic and neutral fractions (as given by relation (5)) entering the solid bulk. After n_c collisions, the emerging fractions $P_f^0(n_c)$ and $P_f^+(n_c)$ are deduced by the following matrix representation:

$$\begin{pmatrix} P_f^0(n_c) \\ P_f^+(n_c) \end{pmatrix} = \begin{pmatrix} 1 & 1-\mathrm{e}^{-(L-x_n)/\lambda_0} \\ 0 & \mathrm{e}^{-(L-x_n)/\lambda_0} \end{pmatrix} \begin{pmatrix} 1-P & P \\ P & 1-P \end{pmatrix} \begin{pmatrix} 1 & 1-\mathrm{e}^{-(x_n-x_{n-1})/\lambda_0} \\ 0 & \mathrm{e}^{-(x_n-x_{n-1})/\lambda_0} \end{pmatrix} \times \begin{pmatrix} 1-P & P \\ P & 1-P \end{pmatrix} \begin{pmatrix} 1 & 1-\mathrm{e}^{-x_1/\lambda_0} \\ 0 & \mathrm{e}^{-x_1/\lambda_0} \end{pmatrix} \begin{pmatrix} P_{in}^0 \\ P_{in}^+ \end{pmatrix}. \quad (9)$$

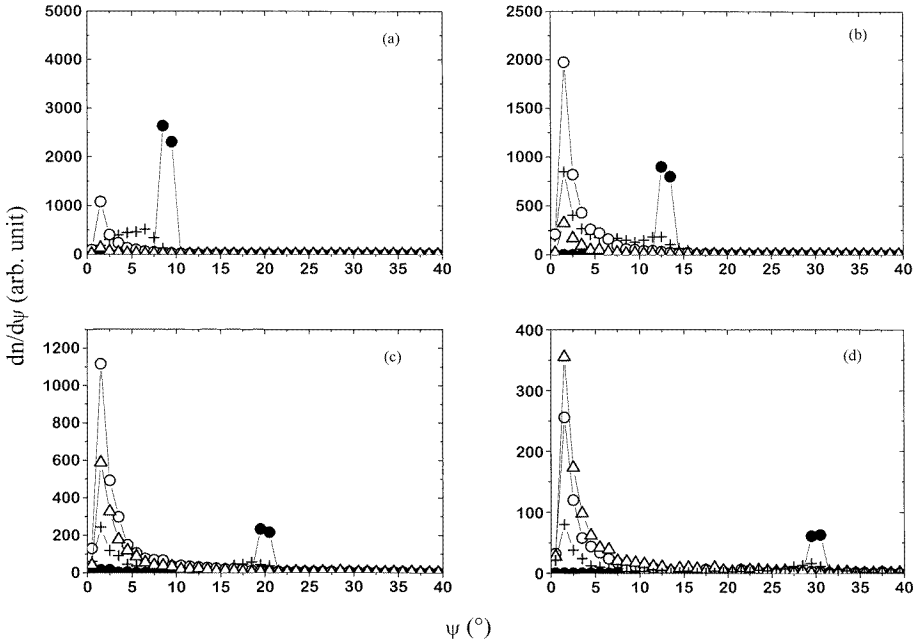

Figure 3. Individual scattering angle distributions for various path lengths: $L = 6$ Å (full circles), $L = 30$ Å (crosses), $L = 150$ Å (open circles) and $L = 306$ Å (up triangles), provided by the modified TRIM code. The total scattering angles are: (a) $\theta = 9°$; (b) $\theta = 13°$; (c) $\theta = 20°$ and (d) $\theta = 30°$ for incidence angle $\alpha = 6°$.

Two types of matrix appear in this relation: one describes the charge commutation by the Auger process between two close collisions and the second the charge commutation by electron promotion during the close collision.

Finally, we calculate a mean evaluation of $\bar{P}_f^0(n_c)$ and $\bar{P}_f^+(n_c)$ from the statistical distribution of the x_i [23].

4.3. Charge fraction

The charge fraction $f^+(\alpha, \beta)$ is evaluated from equation (5) for surface exchange and from statistically averaged equation (9) for charge exchange in the bulk. The probability of emerging from the bulk as an ion is:

$$P_s^+ = \frac{1}{n_t} \int_{L=0}^{\infty} \mathrm{d}L \frac{\mathrm{d}n}{\mathrm{d}L}(\alpha, \beta) \sum_{n_c} \bar{P}_f^+(n_c, L)\Phi(n_c, L) \tag{10}$$

where n_t is the total number of particles scattered in the β direction, $(\mathrm{d}n/\mathrm{d}L)(\alpha, \beta)$ represents the total length distribution and $\Phi(n_c, L)$ is the probability of obtaining n_c close collisions during the total path length L. As n_c increases, the factor $\Phi(n_c, L)(\mathrm{d}n/\mathrm{d}L)(\alpha, \beta)$ decreases strongly and becomes very weak for $n_c > 5$. This is particularly true for small scattering angles (up to $\theta = 30°$). Above this value, more close collisions are necessary for a correct description of the multiple-scattering sequence. However, because of the slowing down, the high values of n_c contribute essentially to the tail of the energy spectra peaks. Then, for the present work, we can restrict ourselves to $n_c \leqslant 5$.

When the Auger neutralization in the vicinity of the surface is taken into account, the charge fraction is:

$$f^+(\alpha, \beta) = P_s^+ \exp(-(a + d)/\lambda_0 \sin\beta). \tag{11}$$

The obtained charge fraction depends on four adjustable parameters: $(a+d)$, λ_0, P_0 and ψ_c. We fit the experimental charge fraction $f^+(6^\circ, \beta)$ for total scattering angles beyond 12°. This limit is estimated by the fact that reionization and neutralization probabilities remain constant above this value (figure 2). Considering that P_s^+ is quite insensitive to β far away from the chosen ψ_c, we obtain a reliable value of: $(a + d)/\lambda_0 \approx 0.0722$. This value corresponds to $v_c \approx 3.6 \times 10^4$ m s^{-1} (equation (1)). The three other parameters are obtained by minimizing the mean least-square deviation of experimental and computed $f^+(6^\circ, \beta)$. Owing to the charge fraction uncertainties, we obtain a similar agreement for several sets of parameters, in the following ranges: $6^\circ < \psi_c < 8^\circ$, 40 au $< \lambda_0 <$ 60 au and $0.3 < P_0 < 0.4$. However, for a given ψ_c, the minimization becomes very sensitive (much more to P_0 than λ_0). If we impose that $\psi_c = 6^\circ$, corresponding to the crossing distance $R_c = 0.35$ Å, the best agreement is found for $\lambda_0 = 40$ au and $P_0 = 0.396$ (figure 4).

4.4. Energy and time of flight distribution

The scattering angle distribution has principally two components (figure 3). The first is constituted by single collision on the near-surface atoms and the second by multiple scattering at larger depth. This multiple-scattering component essentially contains low-angle binary collisions; the nuclear stopping power can then be neglected. The surface atoms scatter the projectile at an energy kE, where k is the kinematic factor and E the initial energy of the projectile. Therefore, the length distribution can be converted to the energy spectra, starting at energy kE, by introducing the inelastic energy loss

$$\frac{\mathrm{d}n}{\mathrm{d}E} = \frac{\mathrm{d}n}{\mathrm{d}L} \frac{1}{(\mathrm{d}E/\mathrm{d}L)_{inel}} \tag{12}$$

where $(\mathrm{d}E/\mathrm{d}L)_{inel}$ is the inelastic stopping power which was calculated in the frame of the density functional theory (DFT) [24] from the transport cross section at the Fermi level. The density of the valence electrons is characterized by the experimental value of the mean electron radius $r_s = 1.97$ au as tabulated by Isaacson [25]. The self-consistent potential and the phase shifts are computed for both He^+ and He^0 by forcing the bound level to be singly and doubly occupied respectively. We found 1.30 as a ratio of ionic to neutral stopping power. This result is very different from the theoretical value 4.45 given by the linear dielectric response theory [13]. It is worth noting that a similar small ratio has been found in DFT by these authors for the H projectile [26].

In order to confirm the assertion (12), the energy distribution obtained by this way is compared with that obtained directly by complete Monte Carlo simulation. The agreement is excellent up to a total scattering angle of 30°. In view of the relatively close value of He^+ stopping power to that of He^0, we adopt that of the neutral one whatever the charge state. The energy loss in the vicinity of the surface outside the bulk is also neglected. Despite the slowing down of the particle in the bulk, the value of the mean length λ_0 and the value of $(\mathrm{d}E/\mathrm{d}L)_{inel}$ are taken as constants. Because a quite small part of the energy spectrum (about 1 keV) is considered, the particle velocity varies only within about 13%, and then this approximation can be considered as valid.

The energy loss in close-encounter reionization is about 20 eV for the He–Si system as expected from ionization energies of the partners and as experimentally found by Shoji *et al* [4]. Assuming that in the neutralization paths, the energy gains have the same order of

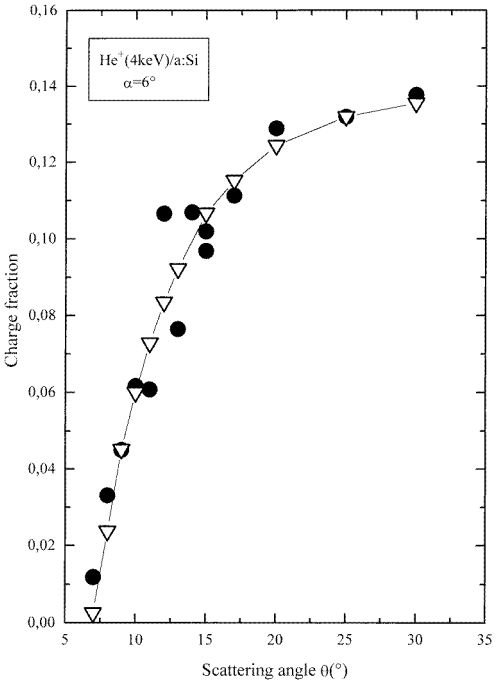

Figure 4. Angular distribution of the experimental charge fraction (full circles) compared to the theoretical one (down triangles) obtained with the following parameters: $\psi_c = 6^\circ$, $\lambda_0 = 40$ au and $P_0 = 0.396$.

magnitude, the total energy transfer for five close collisions (see section 4.3) cannot exceed ± 100 eV corresponding to a TOF shift lower than the 20 ns width of the acquisition channel used here. Therefore, this cause of slowing down has been neglected in our calculation.

The energy distribution of simulated spectra is converted to a TOF spectra by using simple transformations and the features of the spectrometer. For the neutral particles, the TOF distribution is given by:

$$\left(\frac{\mathrm{d}n^0}{\mathrm{d}t}\right)_t = \frac{\mathrm{d}n}{\mathrm{d}L}(\alpha,\beta)\frac{1}{(\mathrm{d}E/\mathrm{d}L)_{inel}}\left(\frac{\mathrm{d}E}{\mathrm{d}t}\right)_t \left\{ \sum_{n_c=0}^{5} \bar{P}_f^0(n_c, L)\Phi(n_c, L) + \left(\sum_{n_c=0}^{5} \bar{P}_f^+(n_c, L)\Phi(n_c, L) \right)(1 - \exp(-(a+d)/\lambda_0 \sin\beta)) \right\}. \quad (13)$$

The first term in the curly brackets is related to the neutral particles emerging from the solid and the second to the particles neutralized in the exit phase.

For the ionic particles, we have:

$$\left(\frac{\mathrm{d}n^+}{\mathrm{d}t}\right)_t = \frac{\mathrm{d}n}{\mathrm{d}L}(\alpha,\beta)\frac{1}{(\mathrm{d}E/\mathrm{d}L)_{inel}}\left(\frac{\mathrm{d}E}{\mathrm{d}t}\right)_t \left(\sum_{n_c=0}^{5} \bar{P}_f^+(n_c, L)\Phi(n_c, L) \right) \times \exp\left(-(a+d)/\lambda_0 \sin\beta\right) \quad (14)$$

where the post-accelerating voltage is taken into account.

Finally, the profiles are convoluted by the apparatus function defined in section 2. The result of these calculations, using the optimized parameters, is shown in figure 5 and

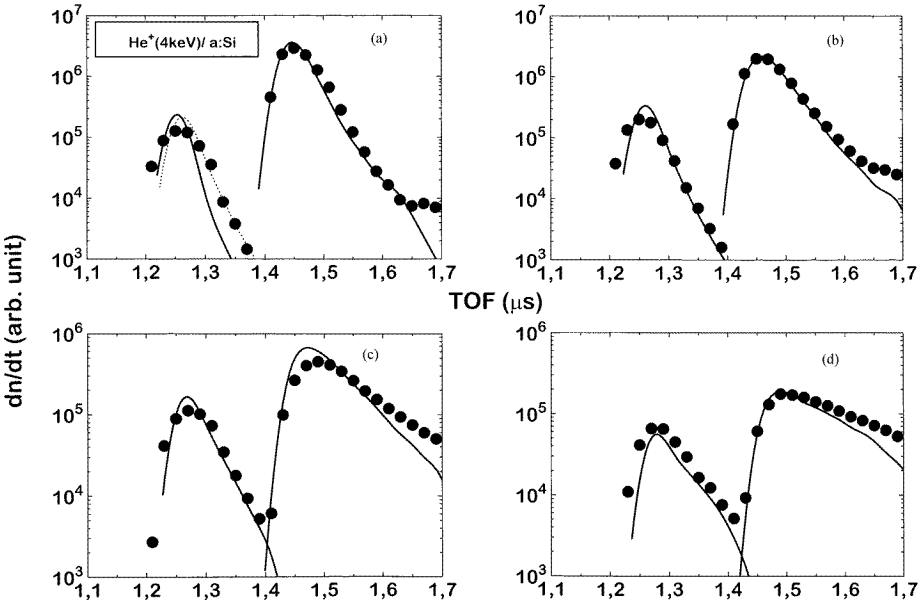

Figure 5. Experimental (full circles) and computed (line) TOF spectra for neutral and ionic He for various total-scattering angles: (a) $\theta = 9^\circ$: dashed line with image effect, full line without; (b) $\theta = 13^\circ$; (c) $\theta = 20^\circ$ and (d) $\theta = 30^\circ$. The incidence angle is $\alpha = 6^\circ$. The used optimized parameters are the same as those of figure 4. The inelastic stopping power is 0.55 times that obtained by DFT computation (see text).

compared to the experimental spectra for various scattering angles. It must be indicated that the normalization of the theoretical data is performed only by comparison of the total yields at $\theta = 10^\circ$. The best fit is found for an electronic stopping power of 0.049 au i.e. 0.55 times that we have computed. This value is very close to the empirical value of ZBL [15]. This point will be discussed later. The general agreement is satisfactory, particularly for the neutral part of the spectra. The slight discrepancy appearing in the tail of the neutral peak when θ increases may be due to the insufficient value used for n_c. For small values of β, the calculated ionic peak is somewhat narrow for $\alpha = 6^\circ$ while it correctly agrees with the experiment for $\alpha = 20^\circ$ (figure 6). This fact can be explained by the image charge effect, which can lead to effective values of incidence angle α_s and exit angle β_s significantly different from the nominal values α and $\beta = \theta - \alpha$. Assuming the image potential given for $r_s = 2$ by Kato *et al* [27], the difference between the actual and nominal angles is higher than 1° up to $\beta = 6^\circ$ for the present experimental conditions. For $\alpha = 6^\circ$, the length distribution $\mathrm{d}n/\mathrm{d}L$ is more dependent on the exit angle β than for $\alpha = 20^\circ$ [23]. Thus, we obtain a better agreement for small values of β without any image effect at $\alpha = 20^\circ$ in comparison with $\alpha = 6^\circ$. For this latter, it is necessary to use the actual angles (α_s, β_s) instead of the nominal ones (α, β) in the length distribution of (14). However, since the neutralization can occur along the incoming path, the increase of incidence angle is less than 1°. Therefore, in practice, the image effect in the entry path is disregarded and only β is corrected. As shown in figure 5(a), this modification clearly improves the agreement with the experimental data, especially in the tail of the ion peak.

Another consequence of the charge image effect can be deduced from the behaviour of the charge fraction as a function of the normal component of exit velocity $v_{out} \sin\beta$.

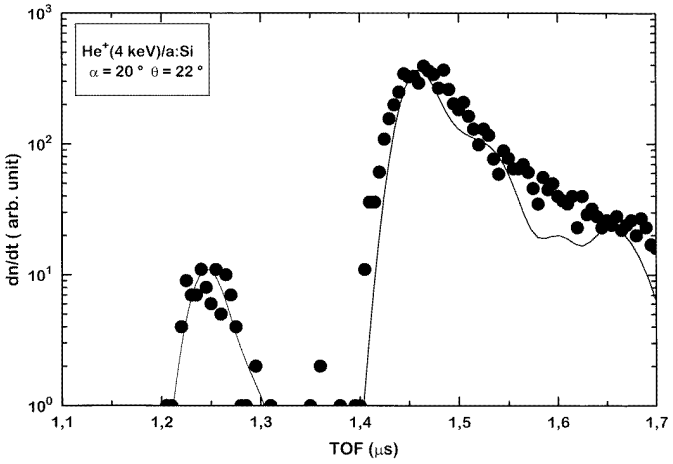

Figure 6. As figure 5 for $\alpha = 20^\circ$ and $\theta = 22^\circ$.

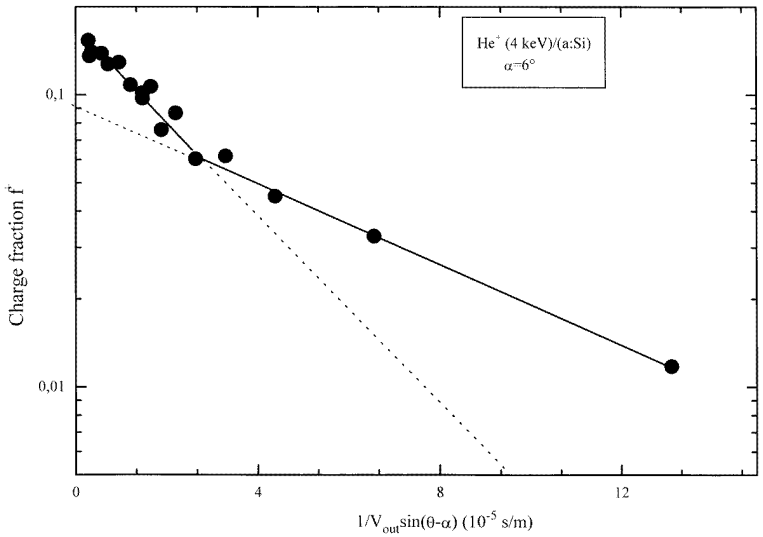

Figure 7. Variation of the charge fraction with the inverse normal component of the detected particle velocity. The two straight lines fit the part $\theta > 13^\circ$ and $\theta < 13^\circ$ respectively.

The curve of f^+ against $1/v_{out} \sin\beta$ (figure 7) presents two linear parts corresponding respectively to large ($\beta > 6^\circ$) and small exit angle ($\beta < 6^\circ$). The ratio of the two slopes is about 2. The image force strongly acts only very near the image plane, i.e. at a distance d from the surface. Then, for small β, the ion path can be approximated by two straight lines characterized by two normal velocities: $v_{out} \sin\beta_s$ for $z < d$ and $v_{out} \sin\beta$ for $z > d$. So, the ion survival probability varies as $\exp(-d/\lambda_0 \sin\beta_s - a/\lambda_0 \sin\beta)$. Because the effective exit angle β_s is nearly constant (3.5–4°) for very low values of β, the ion survival probability depends primarily on $\exp(-a/\lambda_0 \sin\beta)$. For large exit angles, the image effect is negligible and the ion travels outside the bulk with the same normal velocity for both $z < d$ and $z > d$ parts. Then, the ion survival probability varies as $\exp(-(a+d)/\lambda_0 \sin\beta)$. Therefore, the slope ratio given above corresponds to $(a+d)/a$, so that we can deduce $a \approx d$.

5. Discussion

We have noticed the high value of the stopping power obtained by DFT calculation with respect to that experimentally deduced. This important difference can be attributed to the approximation of the free electron gas used for the silicon valence electrons. Indeed, we have in this way neglected the influence of the gap on the excitation process. In the case of the free electron gas, each conduction electron near the Fermi level can be excited whatever the transferred momentum, while this is not the case in a semiconductor. There is a minimum momentum transfer for the top valence electrons to be promoted to the conduction band. This restriction will limit the energy exchange between the projectile and the target electron, so the stopping power will be reduced with respect to a Fermi electron gas. This excitation threshold has been already introduced by Valdes *et al* [28] to explain the deviation from velocity proportionality of the electronic stopping power at low energy.

In our calculation, we consider the same stopping power for both ionic and neutral helium. The disagreement observed in the tail of ion peak at small exit angles may arise from this underestimation of He^+ inelastic energy loss. Moreover, as the ratio between He^+ and He^0 stopping power increases with r_s, our approximation is certainly not valid for $z > d$ and, then, particularly fails for small scattering angles. A more accurate calculation must take into account the two values of stopping power but this requires the knowledge of length distribution of each charge state.

The obtained transition rate τ_0^{-1}, of about 0.005 au, is smaller than the value observed for metal surface with a similar r_s (e.g. 0.014 au for He/Ni [29]) while it is comparable to the 0.006 au found for an insulator (He/LiF [30]). This is consistent with the presence of a gap and the difference between the electronic structures of the valence bands. Knowing λ_0, it is easy to extract $a + d = 2.88$ au and then $a \# d = 1.44$ au. These results are comparable to those of Närmann *et al* [13] in the case of He^+/Ni(110) ($r_s = 1.8$ au) who find $a + d = 2.48$ au. More recently, Winter [31], using both He^0 and He^+ on Al(111) ($r_s = 2.07$), obtains $a = 1.3$ au. Our value of d also agrees with the theoretical value of the image plane point (1.6 au) calculated in the DFT frame [32] for $r_s = 2$.

6. Conclusion

The He^+/a:Si interactions have been studied in this work through the angular behaviour of the He^+ and He^0 scattered TOF spectra. An original numerical model, taking into account the multiple-scattering events and the charge exchange processes, has been elaborated in order to allow a quick adjustment of several parameters. This is made, in a first step, under a few assumptions and approximations which can be reconsidered or refined in a more accurate approach. The sensitivity of the optimization would be improved by a simultaneous fitting of the energy spectra and the charge fraction distribution.

Some results have been deduced. The observed electronic stopping power is smaller than the value expected from the DFT calculation. This discrepancy seems to be linked to the gap of the semiconductor Si. We have shown the close values of the stopping power for He^+ and He^0 as correctly predicted by the DFT contrary to what is expected from the linear dielectric response theory. This leads to an important simplification in the model. The spatial distribution of electronic density in the vicinity of the surface agrees well with the other data available in the literature. The two main processes for charge exchange, Auger neutralization and exchange in close encounter, have been taken into account in the model. The first one is correctly described in the Hagstrum model. The second is considered as a threshold process in a quasi-molecule frame. The obtained value of the mean free

path of Auger neutralization is larger than that measured for metal with the same r_s. The influences of the so-called image charge on the TOF spectra and the angular distribution of charge fraction have been underlined. The importance of this effect for small incidence and exit angles has been clearly shown. A rigorous approach implies an accurate non-linear calculation of the potential image along the particle trajectory.

Acknowledgment

Thanks to Dr M El Bahi (Institute of Mathematics, USTHB) for his appreciable help in the mathematical part of this work.

References

[1] Niehus H, Heiland W and Taglauer E 1993 *Surf. Sci. Rep.* **17** 213
[2] Hagstrum H D 1954 *Phys. Rev.* **94** 336
[3] O'Connor D J, Shen Y G, Wilson J M and MacDonald R J 1988 *Surf. Sci.* **197** 277
[4] Shoji F, Nakayama Y, Oura K and Hanawa T 1988 *Nucl. Instrum. Methods* B **33** 420
[5] Van Leerdam G C, Lenssen K M H and Brongersma H H 1990 *Nucl. Instrum. Methods* B **45** 390
[6] Tsuneyuki S and Tsukada M 1986 *Phys. Rev.* B **34** 5758
[7] Aono M and Souda R 1987 *Nucl. Instrum. Methods* B **27** 55
[8] Barat M and Lichten W 1972 *Phys. Rev.* A **6** 213
[9] Boers A L 1984 *Nucl. Instrum. Methods* B **4** 98
[10] Lacombe S, Esaulov V, Guillemot L, Grizzi O, Maazouz M, Mandarino N and Vu Ngoc 1995 *J. Phys.: Condens. Matter* **7** L261
[11] Rabalais J W, Chen J N, Kumar R and Narayana M 1985 *J. Chem. Phys.* **83** 6489
[12] Beuken J M and Bertrand P 1992 *Nucl. Instrum. Methods* B **67** 340
[13] Närmann A, Schmidt K, Heiland W, Monreal R, Flores F and Echenique M 1990 *Nucl. Instrum. Methods* B **48** 378
[14] Robinson M T and Torrens I M 1974 *Phys. Rev.* B **9** 5008
[15] Ziegler J F, Biersack J P and Littmark U 1985 *The Stopping and Ranges of Ions in Solids* (New York: Pergamon)
[16] Benazeth C, Benoit-Cattin P, Cafarelli P, Reynes P, Ziesel J P and Benazeth N 1994 *Nucl. Instrum. Methods* B **94** 581
[17] Närmann A 1989 *Thesis* Osnabruck University
[18] Sols F 1985 *Thesis* Universidad Autonoma de Madrid
[19] Lorente N, Monreal R and Alducin M 1994 *Phys. Rev.* A **49** 4716
[20] Muda Y and Newns D M 1988 *Nucl. Instrum. Methods* B **33** 388
[21] Sigmund P 1975 *Radiation Damage Process in Materials (Series E 8)* ed C H S Dupuy (Leyden: Nordhoff)
[22] Khalal-Kouache K, Arezki B, Boudjema M, Boudouma Y, Chami A C, Benazeth C and Benoit-Cattin P 1996 *Proc. French-Lebanon Conf. on Material Sciences (Beyrouth, 1996)*
[23] Arezki B 1997 *Thesis* USTHB
[24] Echenique P M, Nieminen R M, Ashley J C and Ritchie R H 1986 *Phys. Rev.* A **33** 897
[25] Issacson D 1975 *NAPS Document* 02698
[26] Narmann A, Schmidt K, Hofner C and Heiland W 1993 *Nucl. Instrum. Methods* B **78** 72
[27] Kato M, Williams R S and Aono M 1988 *Nucl. Instrum. Methods* B **33** 462
[28] Valdes J E, Eckard J C, Lanstcher G H and Arista N R 1994 *Phys. Rev.* A **49** 1083
[29] Narmann A, Heiland W, Monreal R, Flores F and Echenique P M 1991 *Phys. Rev.* B **44** 2003
[30] Hecht T, Auth C, Borisov A G and Winter H 1996 *Phys. Lett.* A **220** 102
[31] Winter H 1993 *J. Phys.: Condens. Matter* **5** 295
[32] Lang N D and Kohn W 1973 *Phys. Rev.* B **7** 3541